<sup>1</sup>W.Margaret
 Amutha
 B.Padmanabhan<sup>2</sup>,
 W. Abitha Memala<sup>3</sup>,
 M.Pushpavalli<sup>4</sup>,
 Mercy Paul Selvan<sup>5</sup>

# Design, Analysis, And Implementation of a Wind-Powered Bridge-Less AC-DC Converter for DC Power Applications



Abstract: - To address issues caused by frequent power supply interruptions, the Research Designs and Standards Organization (RDSO) is exploring an integrated power supply system based on alternative energy sources. The primary objective is establishing a stable and reliable DC power supply for railway signaling installations, which is critical for maintaining uninterrupted train operations. This paper introduces a new wind-powered bridgeless AC-DC converter designed to overcome the limitations of conventional AC-DC boost converters, such as complexity, cost, potential EMI issues, and concerns about component stress and reliability. Before adopting this converter topology, it is essential to assess these factors concerning specific application requirements and constraints thoroughly. The bridgeless boost converter operates through power factor correction (PFC) and DC-DC conversion stages. During PFC, AC input voltage is rectified to achieve a unity power factor, reduce harmonics, and improve compatibility with the utility grid. A Hunting Algorithm (HA) is preferred to extract maximum power. A battery backup ensures continuous operation during wind source unavailability to meet load demands. The system features a power rating of 1 kW, with an input voltage of 96V and an output voltage of -48V. Simulations conducted using MATLAB/Simulink encompass wind characteristics, MPPT tracking, bridgeless converter performance, operational modes, and analysis. Detailed loss calculations are performed to assess efficiency, resulting in an efficiency of 97.6% for the proposed converter with the controller. A prototype model with an input power rating of 1.2kW and output power of 1kW validates simulation results against hardware performance.

Keywords: Bridgeless AC-DC converter Hunting Algorithm (HA) PID controller MPPT tracking Matlab/Simulink

## 1. INTRODUCTION

A dependable and secure power system supports railway operations, including signals, points, interlockings, and communications. The power system must be resilient against failures and deliver a consistent, stable supply to ensure the proper functioning of control and communications equipment. In a signaling system, a constant power supply is required depending upon the signaling system, such as LED Signals, track circuits, Axle Counters, data loggers, indication panels, Visual Display Units (VDU), and Fire Alarm systems. In non-electrified or isolated areas, primary power is typically sourced from conventional power supplies via remote feeders, which are often unreliable regarding availability and voltage stability. Battery backups with chargers are used for all DC circuits, but these setups require extensive maintenance. Frequent supply interruptions cause signal outages until diesel generators can be activated. Additionally, equipment failures, such as those involving battery chargers or transformers, necessitate manual changeover to standby systems, leading to delays in power restoration. An Integrated Power Supply (IPS) system provides a stable and reliable AC and DC power supply to railway signaling installations, ensuring proper train movement despite AC mains variations or interruptions.

Corresponding Author: Dr. W. Abitha Memala

 $Department \ of \ EEE, \ Sathyabama \ Institute \ of \ Science \ and \ Technology, \ Chemancheri, \ Chennai, \ Tamilnadu.$ 

Email: abithamemala.eee@sathyabama.ac.in

Copyright © JES 2024 on-line: journal.esrgroups.org

<sup>&</sup>lt;sup>1</sup>Assistant Professor, EEE, SRM Institute of Science and Technology, Ramapuram, Chennai, margarew@srmist.edu.in,

<sup>&</sup>lt;sup>2</sup> Associate Professor and Head, Adithya Institute of Technology, Coimbatore, padmanabhan4eee@gmail.com.

<sup>&</sup>lt;sup>3</sup> Professor, EEE, Sathyabama Institute of Science and Technology, Chemancheri, Chennai, abithamemala.eee@sathyabama.ac.in.

<sup>&</sup>lt;sup>4</sup>Assistant Professor, EEE, Sathyabama Institute of Science and Technology, Chemancheri, Chennai, pushpavalli.eee @sathyabama.ac.in

<sup>&</sup>lt;sup>5</sup> Professor, CSE, Sathyabama Institute of Science and Technology, Chemancheri, Chennai, mercypaulselvan @gmail.com

As its name suggests, the IPS has been designed and developed to offer comprehensive power solutions, from a single system to all signaling circuits [1],[2].

According to author B. Yang et al. [3] and A.W. Ibrahim et al. [4], the depletion of fossil fuels has spurred a growing interest in renewable energy sources. Wind systems are favored for their environmentally friendly, clean, and energy-efficient alternatives to fuel-driven sets. These systems enhance productivity by providing an uninterrupted power supply. Various strategies, such as perturbation and observation (P&O) and incremental conductance (IC), have been utilized to operate wind systems at maximum power [5], [6]. This work focuses on a wind system utilizing the Hunting Algorithm [HA] for maximum power point tracking (MPPT). Given the intermittent nature of solar PV, energy storage systems like batteries can compensate for power fluctuations. According to authors V.R. Kota et al. [7], E.M. Ali et al. [8], A.K. Podder et al. [9], and R. Guruambeth et al. [10], various DC-DC power converter topologies, including Luo, buck-boost, zeta, SEPIC, and Cuk, are explored to achieve the desired power. Traditional converter topologies may face complexity, cost, potential EMI issues, concerns about component stress, reliability, voltage gain limitation, and reduced output voltage. To address these issues, authors introduce the negative output inverse buck-boost converter [11]- [15]. The Cuk converter is chosen for its high efficiency, reduced switching stress, and high voltage gain [16].

Maintaining constant power in DC converters is challenging, necessitating a controller for stable performance [17]. Previous studies have used proportional-integral (PI) controllers, but these often face peak overshoot issues [18]-[19]. To address these challenges, this paper introduces a novel approach using a tuned proportional-integral-derivative (PID) controller with carefully adjusted tuning gains (Kp, Ki, Kd) [20]. This approach ensures a constant and stable output power with minimal settling time and reduced peak overshoot, even under significant load and input disturbances [21]-[22]. The proposed system supplies the DC voltage to the load, requiring -48V. Key advantages of the proposed work include a hybrid wind system powered DC power applications, eliminating the need for additional sensors for controller necessities [23]-[25]. The involvement of a bridgeless AC-DC converter enables buck/boost capabilities with minimal switching losses. The paper's structure includes an introduction and literature review in section 1, the framework of the proposed system and its basic operation in section 2, various modes of operation of bridgeless AC-DC converter with wind system design in section 3, and optimization methods for the controller in section 4. The overall system is simulated in Matlab/Simulink, and the results are presented in Section 5, followed by discussions and inferences. Finally, section 6 presents the conclusion.

# 2. SYSTEM DESCRIPTION

Figure 1a shows the block diagram of a conventional bridge-less converter for DC power applications. The block diagram comprises a wind energy source, battery storage system, DC load, bidirectional converter, and conventional bridge-less converter. As renewable energy systems are intermittent in nature, energy storage elements are used as a backup.

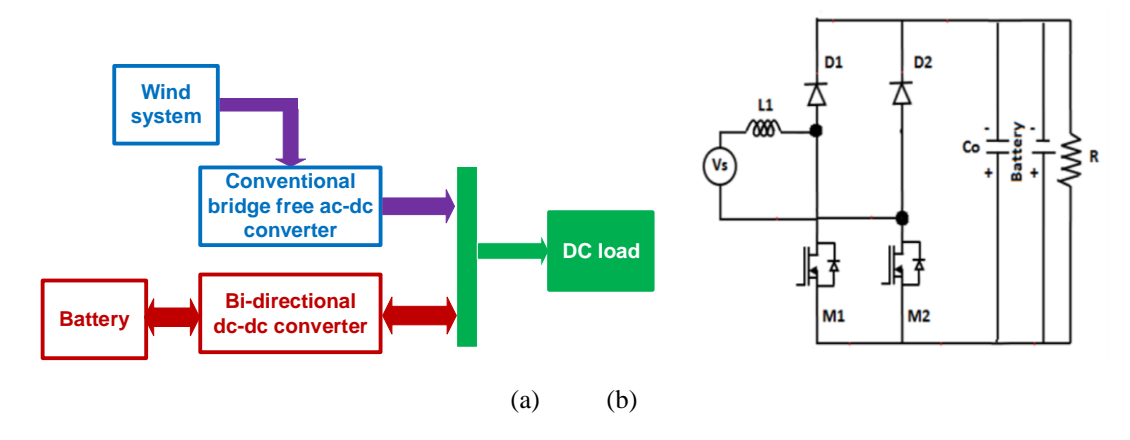


Figure 1. (a) Block diagram of conventional bridge less converter (b) Topology of conventional converter

Battery is used to store energy when the sources are available and can be used whenever needed. The gating of the proposed AC-DC converter is supplied through the PWM generator. The converter synchronizes the sources and the load, thereby regulating the output voltage. The wind source can efficiently power loads, storing surplus energy in batteries using bidirectional DC-DC converters. The hunting algorithm-based PWM pulses achieve maximum power tracking from the wind source. The topology of the conventional wind system-powered DC power load application is shown in Figure 1b.

The working principle of a conventional bridge-less AC-DC converter is similar to that of a common boost converter. In this configuration, current flows through only one diode and one switch at a time. In the design of converter components, duty cycle ratios  $D_{M1}$  and  $D_{M2}$  determination, finding the component values inductor  $L_1$  and output capacitor  $C_0$  is important. In addition, selecting components  $D_1$  and  $D_2$  and M1 and M2 is also essential. It is discussed in the following sections. The design of a conventional bridgeless boost converter is as follows.

$$D_{M1} = \frac{(v_0 - v_{in-mim}) * \sqrt{2}}{v_0} \tag{1}$$

$$D_{M2} = \frac{(V_0 - V_{in-max}) * \sqrt{2}}{V_0} \tag{2}$$

$$L_1 = \frac{V_{in-mim}*\sqrt{2}*D_{M_1}*T_S}{\Delta i_{Lmax}}$$
(3)

$$\Delta i_{Lmax} = \frac{P_0 * \sqrt{2} * 0.3}{V_{in-mim} * \eta * D_{M_1}}$$
(4)

$$C_0 = \frac{2 * P_0}{\left(v_0^2 - \left(0.75 * V_0^2\right)\right) * F_L} \tag{5}$$

Where,

-Duty cycle ratio of the switches M<sub>1</sub> & M<sub>2</sub>  $D_{M1}$  and  $D_{M2}$ - Output voltage Vin-max -Minimum input voltage Vin -max-Maximum input voltage  $F_{L}$ -Line frequency -Efficiency η Ts  $P_0$ - Output power -Switching time (ON/OFF)  $\sqrt{2*V_{in-mim}}$  &  $\sqrt{2*V_{in-max}}$  $V_{M1} & V_{M2}$ V<sub>D1</sub> & V<sub>D2</sub>-V<sub>0</sub>

The conventional bridgeless boost converter has different modes of operation depending on the conducting states of power switches  $M_1$  and  $M_2$ . Figure 2a shows these modes of operation. The working principle of the converter's various modes of operation is explained below.

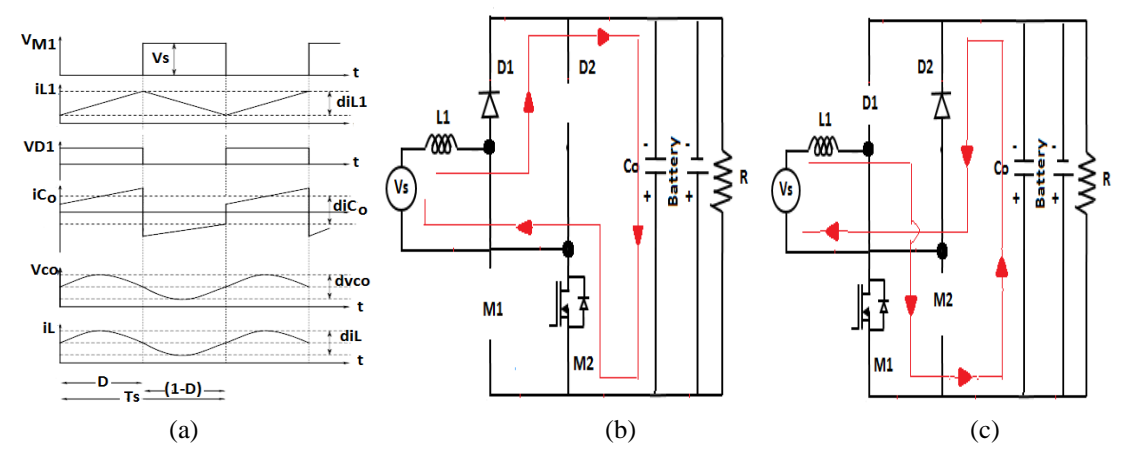


Figure 2. (a) Modes of operation (b) Mode 1 during the positive half cycle (c) Mode 1 during the negative half cycle

To analyze the operation of the converter, it is divided into two parts: one during the positive half-cycle of the input signal and the other during the negative half-cycle. These processes are explained in the following sections.

# 2.1 Positive half cycle of the conventional converter

Figure 2b shows the topology of the converter when the AC input voltage goes positive, whereas Figure 2c shows the topology when the AC input voltage goes negative half cycle. Switch  $M_2$  is in the ON position or high when the input voltage (Vs) increases positively. During this mode, current flows from the input through the inductor  $L_1$ , diode  $D_2$ , and capacitor  $C_0$  storing energy. Capacitor  $C_0$  is connected to the battery, and the DC load is on the output side. Inductor  $L_1$  charges the battery during this mode, feeding the DC load.

# 2.2 Negative half cycle of the conventional converter

Figure 2c shows the topology when the AC input voltage goes negative in the half cycle. Switch  $M_1$  is in the ON position or high during input voltage (Vs) increases in a negative direction. During this mode, current flows from the input through the capacitor  $C_0$ , diode  $D_1$ , inductor  $L_1$ . Capacitor C0 is connected to the battery, and the DC load is on the output side. Capacitor C0 charges the battery during this mode, feeding the DC load. In this topology, two Power MOSFETs are synchronously driven.

#### 2.3 Simulation results of conventional converter

As per the simulation parameters mentioned in Table. 1, the simulation has been run using Matlab/Simulink software.

Simulation parameters Inductors 1mH Capacitors  $C_0$ 440µF Load DC 1 kW Frequency 50KHz **Battery** 100V, Storage 200Ah Switches M<sub>1</sub>& M<sub>2</sub> **MOSFET** 

Table. 1. Simulation parameters of conventional converter

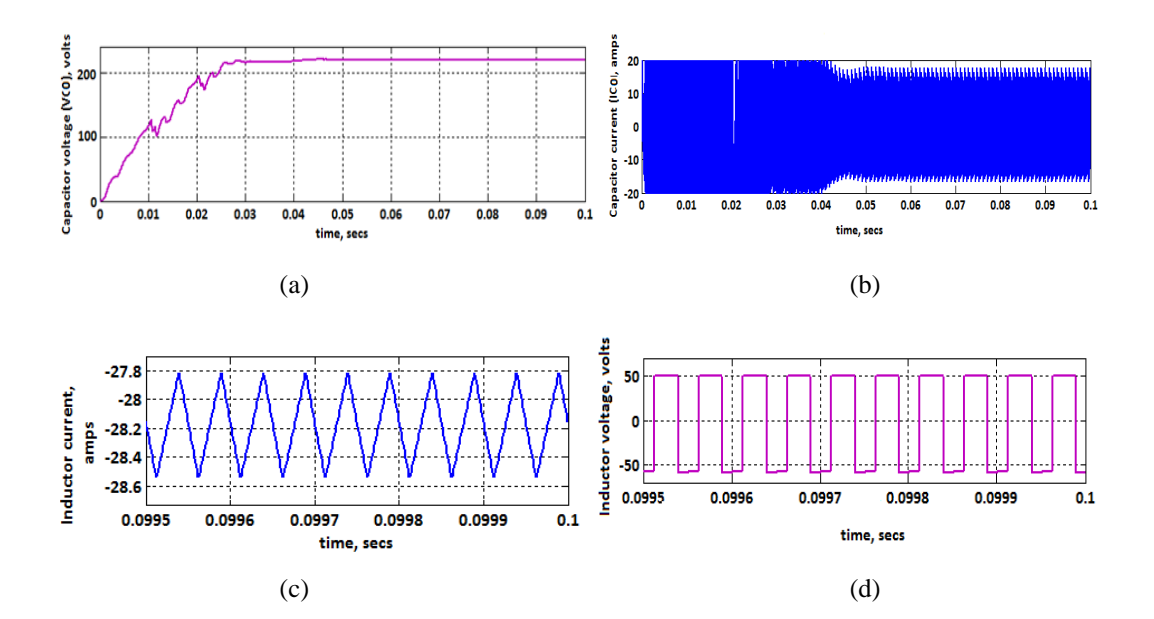


Figure 3e shows the DC output voltage. The voltage obtained at the DC link point is 200V.

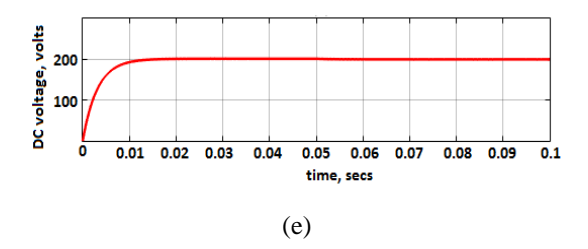


Figure 3. (a) Voltage across the capacitor (b) Current through the capacitor (c) Inductor voltage (d) Inductor current (e) DC output load voltage

The same simulation parameters are also followed for the proposed converter. Figure 3a and Figure 3b show the voltage and current through the capacitor in a conventional bridgeless boost converter. From Figure 3b, the current ripple of the capacitor C<sub>0</sub> is calculated as 19.93%. Figures 3c and 3d depict the inductor voltage and current of the conventional bridgeless boost converter. From the Figs 3c and 3d, it is found that the current ripple of the inductor is 9%. The total losses are calculated as 258.89 watts. The output power is 900 watts. The efficiency of the conventional converter is calculated as 91.83%. A powered AC-DC converter aims to overcome the drawbacks of traditional converter designs and improve the efficiency and performance of high-voltage conversion for DC microgrid applications.

#### 2.4 Block diagram of the proposed converter

Figure 4a illustrates the proposed system, which includes a wind source utilizing the Hunting Algorithm (HA) for maximum power point tracking, a bridgeless AC-DC converter with minimal ripple and switching losses, a battery energy storage component with a bidirectional converter, and a DC load.

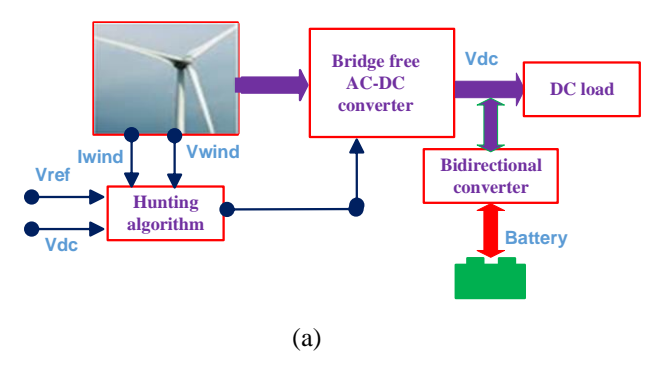


Figure 4. (a) Block diagram of bridge less AC-DC converter

The topology of the proposed wind system-powered DC power load application is shown in Figure 4b.

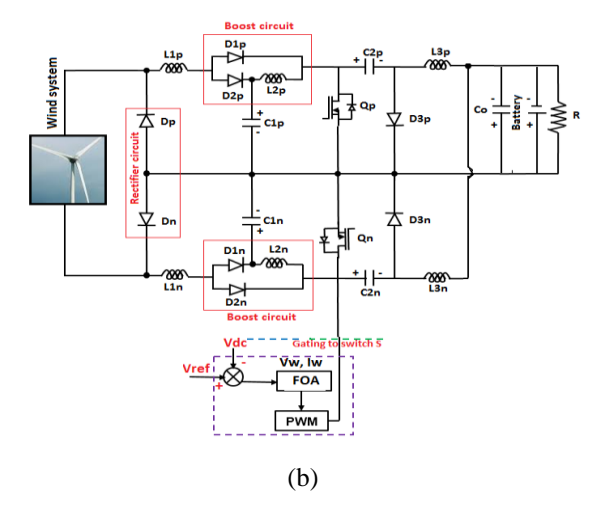


Figure 4. (b) Circuit diagram of bridge less AC-DC converter

The proposed system has various components, such as a wind system, AC-DC converter, Hunting algorithm, PWM controller, battery, and DC load. It is constructed by connecting a conventional boost converter and a bridgeless Cuk converter, thus forming an improved bridgeless Cuk converter. A conventional boost circuit has two diodes (D1P, D2P) and an inductor L2P with a positive input half cycle. During the negative input half cycle of the boost circuit, diodes ( $D_{1n}$ ,  $D_{2n}$ ) and an inductor  $L_{2n}$  are connected. The diodes Dp and Dn acts as a rectifier circuit.

# 2.5 Modelling of the wind system

The WES has a turbine and a PMSG (permanent magnet synchronous generator). A wind turbine captures electrical energy and converts captured wind power. The mechanical power extracted from is,

$$P_{\text{wt}} = \frac{1}{2} \rho A_{\text{w}} V_{\text{w}}^{3} C_{\text{p}}(\lambda, \beta)$$
(6)

 $^{\text{C}}_{\text{p}}$  is the wind speed,  $^{\text{A}}_{\text{w}}$  is the area swept by rotor blades,  $^{\text{(}\lambda,\beta)}$  are the turbine speed and the pitch angle,  $^{\text{V}}_{\text{w}}$  is the wind velocity. The proposed AC-DC converter has a rectifier circuit topology that converts AC to DC voltage. Table 2 gives the parameter specifications of WES.

Parameter		Wind system	
Rated V, speed	I,	100V, 10A, 1850 rpm	
Maximum power		1000 watts	
Wind speed		12 m/s	
Generator		PMSG	

Table. 2. Specifications of wind system

The simulation results of voltage, current, and power of WES are shown in Figure 5.

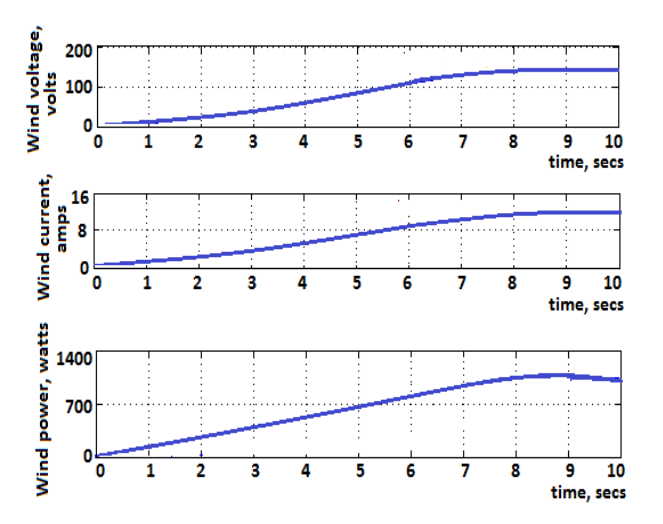


Figure. 5 Wind voltage, current, and power

The simulation result shows that the obtained wind voltage, wind current, and power are 100V, 10A, and 1000 watts, respectively.

#### 2.5 Procedure for Hunting Algorithm

The Hunting Algorithm (HA), inspired by the foraging behavior of whistling kites, black kites, and brown falcons, demonstrated exceptional performance in a numerical study using 233 mathematical test functions. The evaluation covered dimensions ranging from 2 to 100 and involved 150,000 function evaluations. Comparative analyses with 10 classical and contemporary metaheuristic algorithms were conducted using various statistical tests. HA proved its effectiveness in the Competitions on Evolutionary Computation (CEC) 2020, outperforming other algorithms in bound-constrained and real-world optimization problems. The algorithm's capabilities extended to real-size structural frames, surpassing previously developed metaheuristics.

Identify Falcons and Prey in the search space.

Calculate the total distance between the Falcons and Preys.

Define the territory of the Falcons by dispersing the prey.

For each iteration (6) up to n, determine the new positions of Falcon using equation (7)

$$F_l^{\text{new}} = F_l + ((r_1 * GB) - r_2 * F_{\text{near}})$$
  $l = 1, 2 ... n$  (7)

Where,

 $F_l^{new}$  - New position vector of the lth Falcon ( $F_l$ )

GB - Global best

F<sub>near</sub> - Other Falcon in the search space

<sup>r</sup><sub>1</sub> & <sup>r</sup><sub>2</sub> - Uniformly distributed random number in the range of (0,1)

For q=1:r

Calculate the safe under 1th Falcon territory by eq. (8),

$$SP_{l} = \frac{\sum_{q=1}^{r} PR_{q}}{r}, \qquad \begin{cases} q = 1, 2 \dots r \\ l = 1, 2 \dots n \end{cases}$$
 (8)

Determine the new position of the prey by eq. (9),

$$PR_q^{\text{new}} = PR_q + ((r_3 * F_l) - r_4 * SP_l) \begin{cases} q = 1, 2 \dots r \\ l = 1, 2 \dots n \end{cases}$$
(9)

Calculate the safe place outside the 1th Falcon territory by eq. (10),

$$SP_{l} = \frac{\sum_{q=1}^{r} PR_{q}}{r}, \qquad \begin{cases} q = 1, 2 \dots r \\ l = 1, 2 \dots n \end{cases}$$
 (10)

Determine the new position of the prey by eq. (11),

$$PR_q^{\text{new}} = PR_q + ((r_5 * F_{Alter}) - r_6 * SP) \begin{cases} q = 1,2 \dots r \\ l = 1,2 \dots n \end{cases}$$
(11)

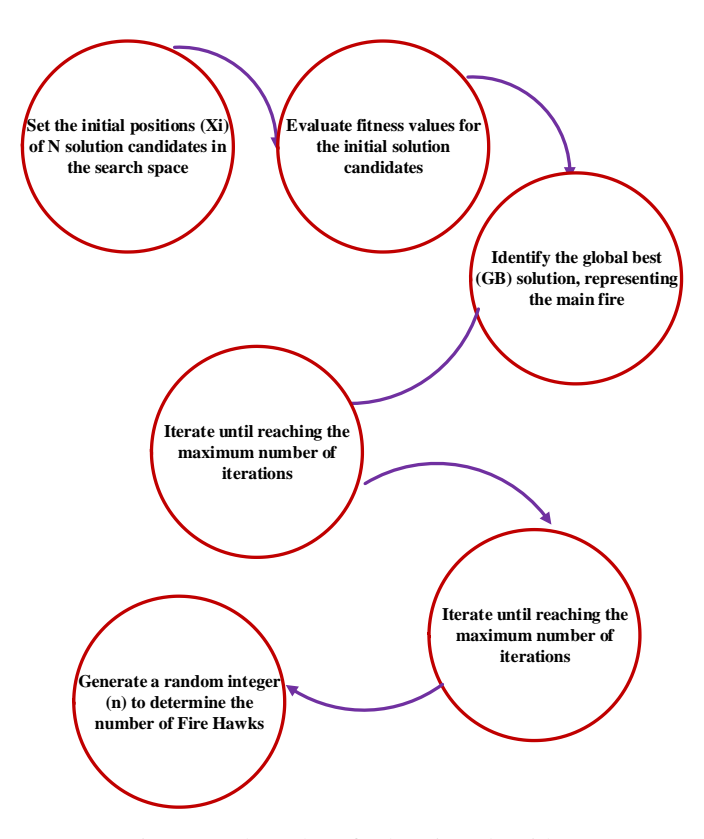


Figure 6. Flow chart for hunting algorithm

Where,

SP -Safe place outside the lth Falcon's territory

F<sub>Alter</sub>- Falcon in the search space

Evaluate fitness values for the newly created Falcons and preys

Determine the GB solution as the main fire

End while

Return GB

End procedure

The above figure illustrates,

$$D_k^1 = \sqrt{(X_2 - X_1)^2 - (Y_2 - Y_1)^2} \begin{cases} k = 1, 2 \dots m \\ l = 1, 2 \dots n \end{cases}$$
 (12)

Where

 $\mathsf{D}^1_k$  - Total distance between the lth falcon and the kth

Prey

M - Total number of prey in the search space

n - Total number of falcons in the search space

 $(X_1, Y_1)$  and  $(X_2, Y_2)$  represent the coordinates of the Falcons and prey in the search space.

# 2.6 Modelling of Battery

The battery capacity (C<sub>b</sub>) is calculated as follows,

$$C_b = \frac{\text{Total watts} * \text{ hours used by the load} * \text{no of days}}{\text{Battery efficiency} * \text{Depth of discharge} * \text{Battery voltage}}$$

$$C_{b} = \frac{1024 * 12 * 0.5}{0.85 * 0.8 * 320} = 28Ah$$
(13)

The charging current (I<sub>batt</sub>) of the battery is

$$0.1*C_b=0.1*28=2.8 A$$
 (14)

Battery discharging = 
$$0.05 * C_b = 0.05*28=1.4A$$
 (15)

Figure 7 shows the simulation results for the battery's voltage, current, and power. These results indicate that the battery voltage is 50V, the current is 10A, and the state of charge (SOC) is 94%.

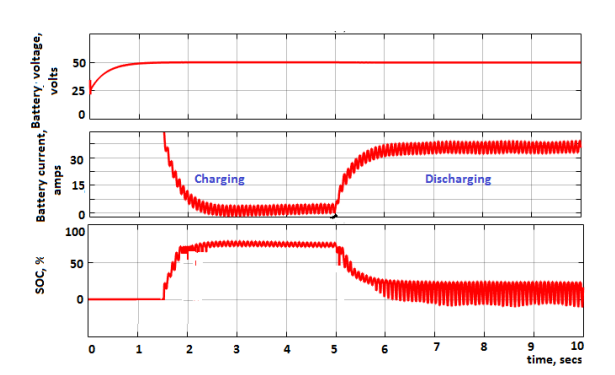


Figure 7. Battery voltage, current, and SOC

# 2.7 Design parameter of proposed ac-dc converter

The design parameters and design equations of the AC-DC converter are given below. Based on the ON/OFF positions of the switch, it is categorized into two states as shown in Figure 7. (a) Switch ON state and (b) Switch OFF state. The converter design can be obtained by using the following formula. Let,

$$L_{1p} = L_{1n}, L_{2p} = L_{2n} \tag{16}$$

$$C_{1p} = C_{1n}, C_{2p} = C_{2n}$$
 (17)

$$L_{1} = \frac{V_{S^{*}} d_{1}}{\Delta I_{L_{s}} * F_{s}} = 1 \text{mH}$$
 (18)

$$L_2 = L_3 = \frac{V_S * d_2}{2*\Delta I_{L_2} * F_S} = 100 \ \mu H \tag{19}$$

$$C_1 = C_2 = \frac{I_0 \cdot d_1}{\Delta V_{C_1} \cdot F_s} = 0.8 \,\mu\text{F}$$
 (20)

$$C_0 = \frac{P_0}{4 * \pi * \Delta V_{C_0} * P_s * V_0} = 440 \ \mu F \tag{21}$$

Applying the volt-sec balance equation on inductor L<sub>1</sub>,

$$V_{C_1} * \left(\frac{1}{2*L_1}\right) - V_S * \left(\frac{1}{L_1}\right) = 0$$
 (22)

It can be written as,

$$V_{C_1} * (\frac{1}{2}) = V_S \text{ or } V_{C_1} = 2 * V_S$$
 (23)

It can be written as,

$$V_{C_2} * d_1 = V_{C_0} \text{ or } V_{C_2} = \frac{V_{C_0}}{d_1}$$
 (24)

Solving the equations

$$V_{C_0} = -V_S * \frac{(2-d_1)*d_1}{(1-d_1)}$$
 (25)

Applying the amp-sec balance equation on capacitor  $C_1$ ,

$$I_{L_1} * \left(\frac{-1}{C_1}\right) + I_{L_2} * \left(\frac{-1}{C_1}\right) = 0$$
 (26)

It can be written as,

$$I_{L_1} = I_{L_2} \tag{27}$$

Applying the amp-sec balance equation on capacitor  $C_2$ ,

$$I_{L_2} * \left(\frac{1}{C_2}\right) + I_{L_3} * \left(\frac{1-d_1}{C_2}\right) = 0$$
 (28)

$$I_{L_3 = -I_{L_2}}$$
 (29)

Applying the amp-sec balance equation on capacitor Co,

$$I_{L_3} * \left(\frac{1}{C_0}\right) + I_{L_3} * \left(\frac{1}{C_0}\right) - V_{C_0} * \left(\frac{1}{R*C_0}\right) = 0$$
 (30)

Solving the equations

$$I_0 = \frac{v_{c_0}}{R} = I_{L_1} * \frac{1}{(1-d_1)} + I_{L_2} * \frac{1}{(1-d_2)}$$
 (31)

Figures 7a to 7d represent the working of various modes.

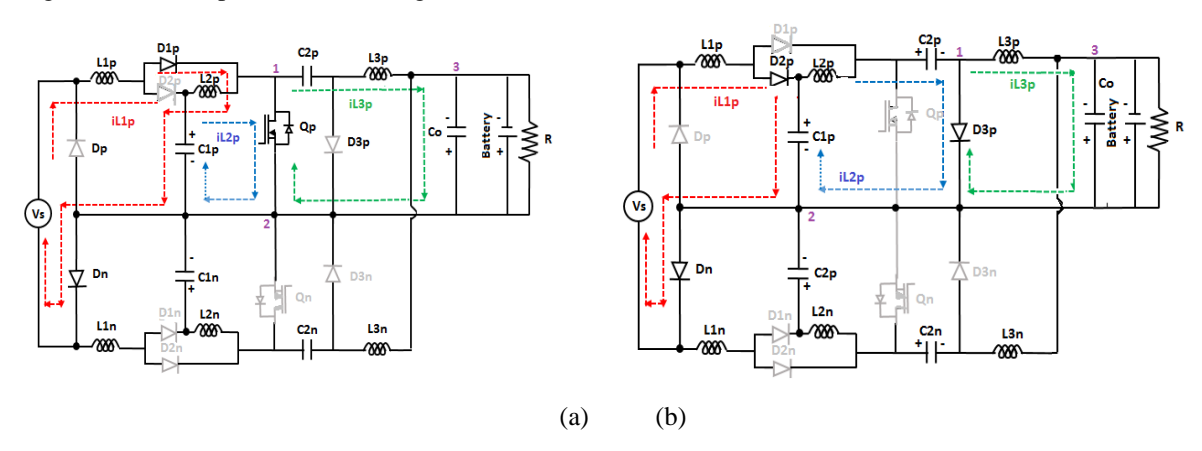


Figure 7 (a) Mode-1 (Qp-ON, Qn-OFF) (b) Mode-2 (Qp-OFF, Qn-OFF)

(During the positive half line of the input)

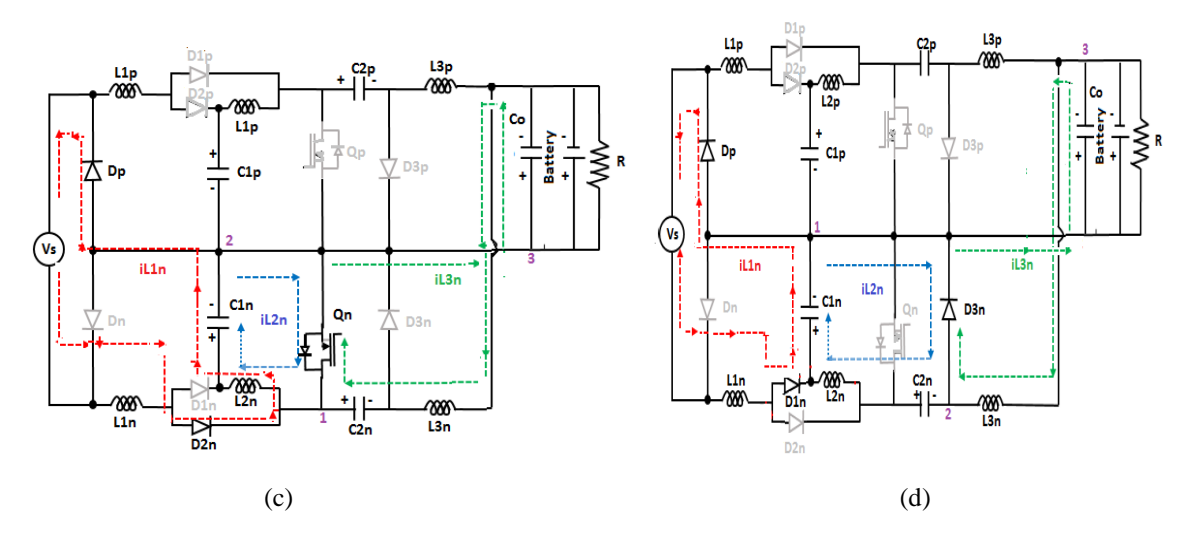


Figure 7. (c) Mode-3 (Qp-OFF, Qn-ON) (d) Mode-4 (Qp-OFF, Qn-OFF)

(During negative input half cycle)

Figure 8 shows the pictorial representation of modes of operation. Table 3 shows the various working modes of the proposed ac-dc converter.

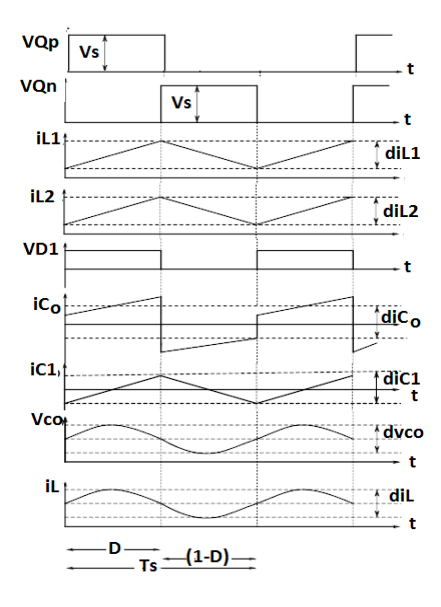


Figure 8. Modes of operation

Table. 3. Modes of operation

Modes	<b>Active lines</b>	Working
1	Qp-ON	During the positive half-cycle of the input, diodes D <sub>P</sub> and D <sub>1P</sub> are
	Qn-OFF	forward-biased. Inductors $L_{1P}$ and $L_{2P}$ charge capacitor $C_{1P}$ . Inductor
		$L_{3P}$ energizes capacitors $C_{2P}$ and $C_0$ , supplying power to the load.
2	Qp-OFF	During the positive half-cycle of the input, diodes $D_n$ and $D_{1P}$ are
	Qn-OFF	forward-biased: Inductors $L_{1P}$ and $L_{2P}$ charge capacitor $C_{1P}$ . The energy from capacitor $C_{1P}$ is transferred to capacitor $C_{2P}$ . Inductor $L_{3P}$ energizes $C_{O}$ , thereby supplying power to the load. The battery

3	Qp-OFF	During the negative half-cycle of the input, diodes $D_P$ and $D_{2n}$ are
	Qn-ON	forward-biased. Inductors $L_{1n}$ and $L_{2n}$ charge capacitor C1n. The
		energy from capacitor $C_{1n}$ is used to energize inductor $L_{2n}$ . Inductor
		$L_{3n}$ and capacitor $C_{2n}$ then energize $C_0$ , supplying power to the load.
		The battery can meet any additional power demand, and excess
4	Qp-OFF	During the negative half-cycle of the input, diodes D <sub>P</sub> , D <sub>2n</sub> , and D <sub>3n</sub>
	Qn-OFF	are forward-biased. Inductors $L_{1P}$ and $L_{2P}$ charge capacitor $C_{1P}$ ,
		while the energy from capacitor $C_{1n}$ is transferred to capacitor $C_{2n}$ .
		Inductor $L_{3n}$ energizes $C_0$ , thereby supplying power to the load. The

# 3. SIMULATION RESULTS AND DISCUSSION

With the below-mentioned parameters in Table. 4, the proposed system is simulated with a hunting algorithm using MATLAB Simulink. It is used to understand the topology thoroughly and the control algorithm better.

Table. 4. Simulation specifications

Parameter	Rating
Input dc voltage	100V
Input power	1200W
Input current	12A
Output voltage	48V
Output power	1000W
Output current	23A
Inductor L <sub>1</sub>	1476 μΗ
Inductors $L_2 = L_3$	1450 μΗ
Capacitors $C_1 = C_2$	0.8 uF
Capacitor C <sub>O</sub>	440 μF
Switching frequency	50 kHz
Resistor R <sub>L</sub>	2.32 Ω

Table. 5 shows the Kp, Ki, and Kd values obtained from the simulation using the hunting algorithm.

Table. 5. Optimized parameters from the HA algorithm

Parameter	Without controller	HA
Proportional(K	9.09	3.92
Integral (Ki)	6.132	0.000

Figures 9a and 9b show the DC link voltage, input voltage, current, and power with and without the controller algorithm. The figures show that the obtained DC voltage is -48V and the current is 20.8A; the obtained power is 1020 watts. It is also seen that the input voltage of 100V and current of 10A is maintained. Then, the THD of 1.12% is obtained with 16th harmonic order. Figure 10 shows the duty cycle of Qp and Qn switches. The duty cycle of 10% and 50 % is maintained at the switches. Figures 11a, 11b, and 11c present the DC voltage, current, and DC power across the load. From the DC output voltage waveform, it is understood that the ripple factor is comparatively low.

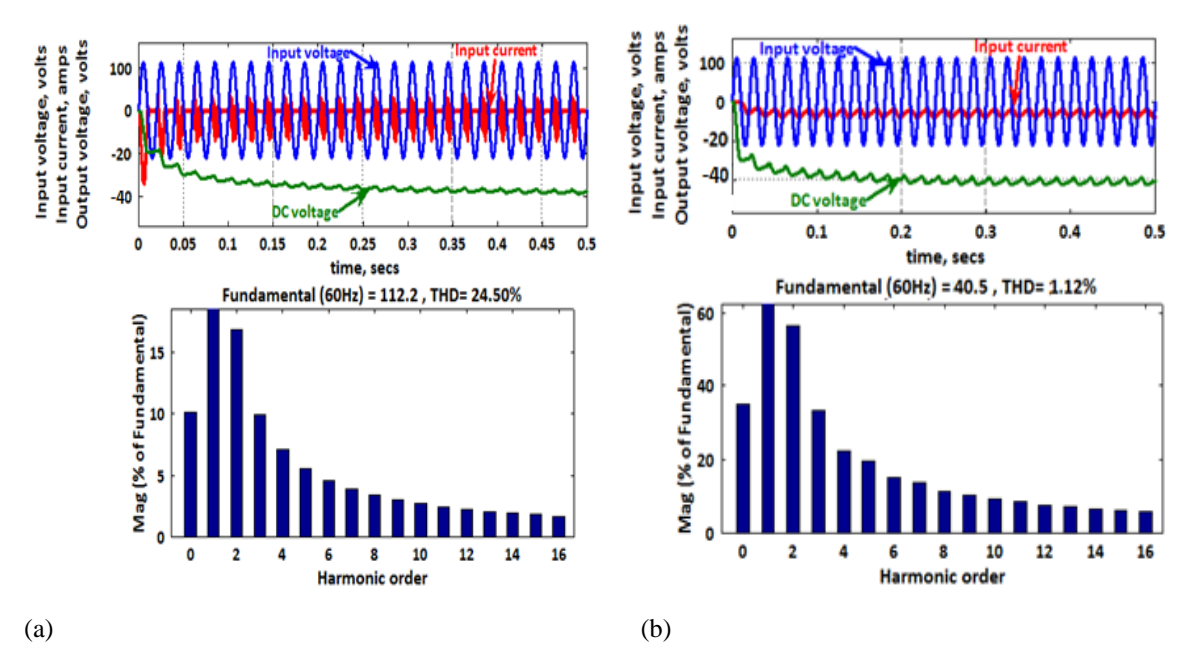


Figure 9. (a), (b) Input and output voltage, current, and power without and with controller and THD

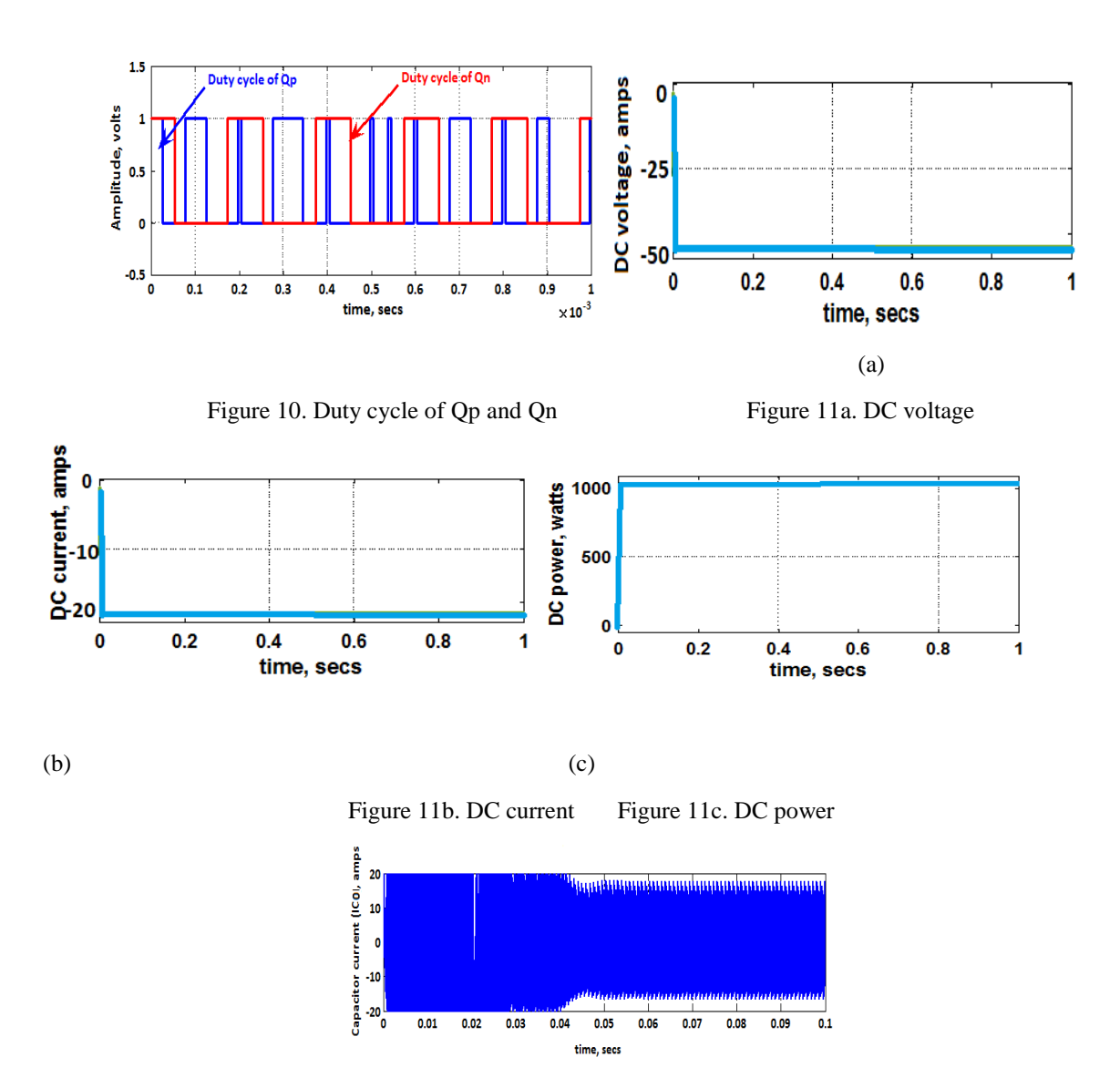


Figure 12. Capacitor current

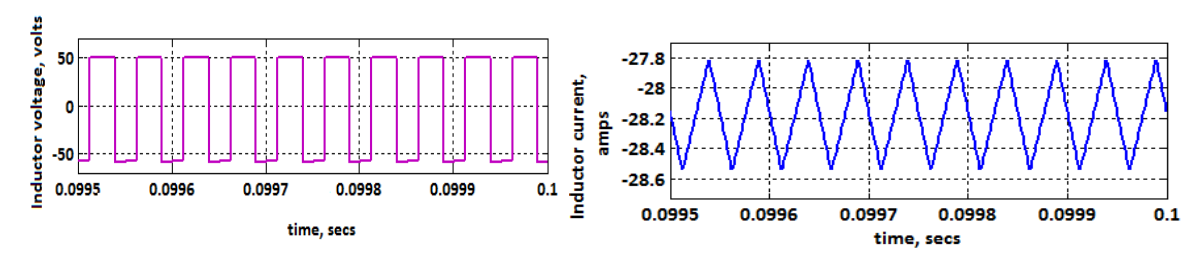


Figure 13. Inductor voltage

Figure 14. Inductor current

Figure 12 depicts the current through the capacitor in the proposed converter. From the figure, it is evident that the current ripple of capacitor C0 is 19.93%. Figures 13 and 14 depict the Inductor voltage and current. From these figures, it is clear that the inductor's current ripple is 9%. The total losses are calculated as 258.89 watts. The output power is 1000 watts. So, the efficiency is calculated as 97.6%.

## 4. HARDWARE IMPLEMENTATION

A wind-powered AC-DC cuk converter with a hunting algorithm tuned to the MANFIS controller using the FPGA-Mojo-3 controller is implemented in real-time. The hardware results are noted down using DSO-X-2002A key sight technology. The proposed topology is tested using the same power and parameters used in the simulation as in Table 5. Figure 15 shows the improved bridgeless cuk converter setup with the FOA algorithm tuned to the MANFIS controller. Figures 16a and 16b show the output voltage and current.

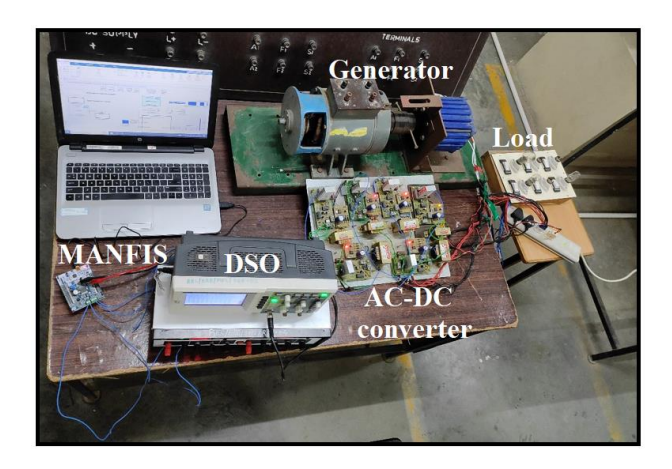


Figure. 15. Improved bridgeless cuk converter

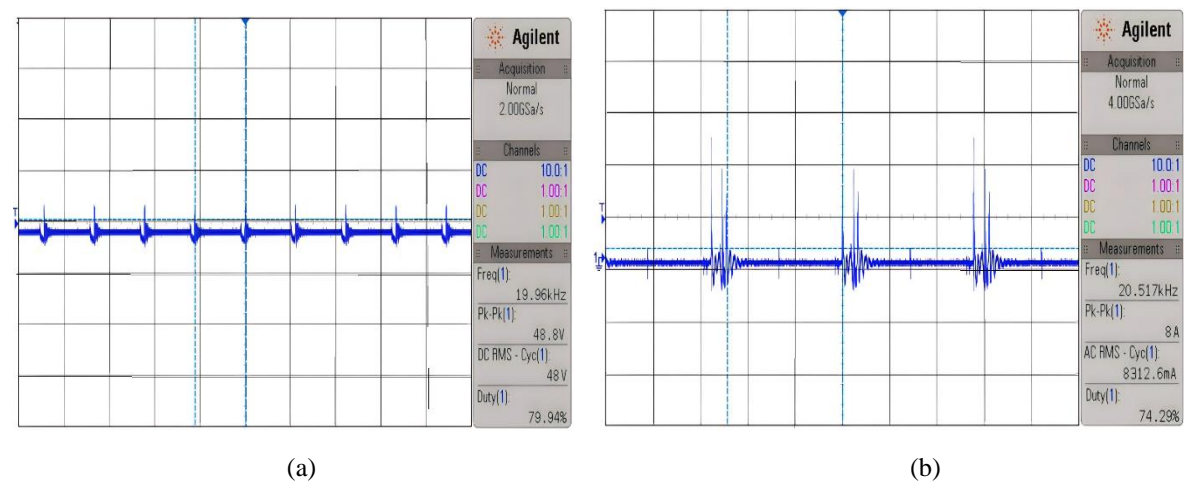


Figure 16. (a) Output voltage, (b) Output current

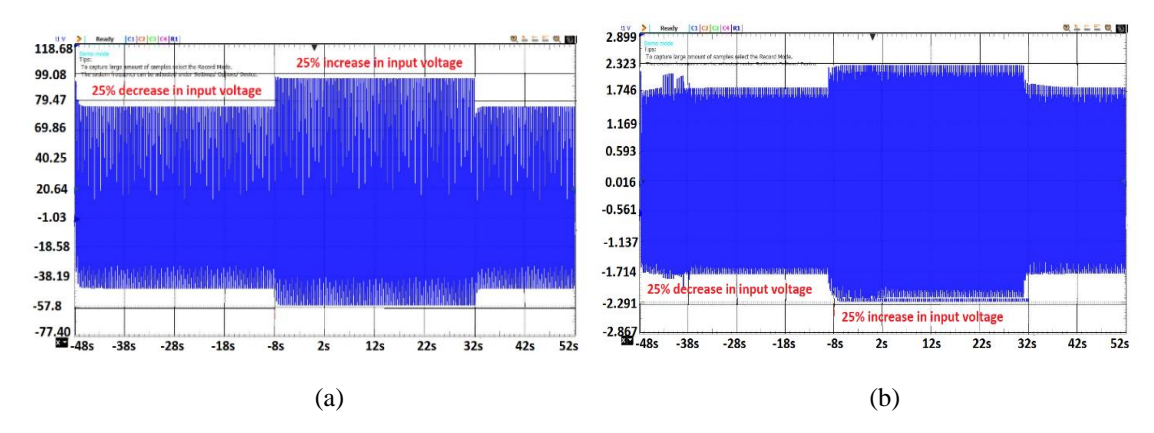


Figure 17. (a) Input voltage with Increase/decrease in input voltage variations (b) Input current with Increase/decrease in input voltage variations

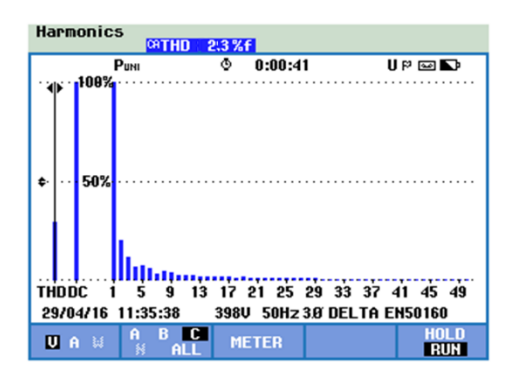


Figure 18. THD of line voltage

Figures 17a and 17b represent the hardware results of input voltage and current waveforms for a 25% increase and decrease in reference voltage. Figure 18 depicts the THD spectrum of a line voltage waveform measured using a Fluke power quality analyzer. The THD obtained is 2.3%. The hardware results show that the output waveforms are well-regulated and have a faster response with small overshoot and minimal settling time.

#### 5. CONCLUSION

This paper introduces a new strategy employing the Hunting Algorithm for tracking the maximum wind power used for DC power applications. The drawbacks of lower convergence speed and steady-state oscillations associated with conventional optimization techniques were addressed through the HA. A wind-powered bridgeless cuk converter has been proposed. It has the advantages of less ripple, high power density, reduced switching losses, and simple structure. The efficiency of the conventional bridge less cuk ac-dc converter and the proposed ac-dc converter is found. A battery backup has also been integrated when the wind source is unavailable, ensuring the load demand. The converter output voltage is directed to the load. The overall system has a power rating of 1kW, input voltage of 96V, and output voltage of -48V. Simulations were carried out using MATLAB/SIMULINK, and the results were presented. Simulation results encompass wind characteristics, MPPT tracking new bridge less converter performance, modes of operation, and its analysis. Elaborate element-wise losses were calculated to find the efficiency and were reported. The obtained efficiency of the proposed converter with the controller was 97.6%. The results obtained are validated with the hardware results.

## REFERENCES

- 1. Tiwari. S.K., Singh. B and Goel. P.K, "Design and control of microgrid fed by renewable energy generating sources", IEEE Transactions on Industry Applications, Vol. 54, No. 3, pp.2041-2050, 2018.
- Revathi, B. Sri and M. Prabhakar. "Solar PV Fed DC Microgrid: Applications, converter selection, design and testing." IEEE Access 10, pp. 87227-87240, 2020.
- 3. Narayanan, Vivek, Seema Kewat and Bhim Singh. "Solar PV-BES based microgrid system with multifunctional VSC."

- IEEE Transactions on Industry Applications, Vol. 56, No. 3, pp. 2957-2967, 2020.
- 4. Kumar, Rajan and Bhim Singh. "Single stage solar PV fed brushless DC motor driven water pump." IEEE Journal of Emerging and Selected Topics in Power Electronics, Vol. 5, No. 3, pp.1377-1385, 2017.
- 5. Wang, Yuanfei, Ping Luo, Xiao Zeng, Dingming Peng, Zhaoji Li and Bo Zhang. "A neural network assistance AMPPT solar energy harvesting system with 89.39% efficiency and 0.01–0.5% tracking errors." IEEE Transactions on Circuits and Systems I: Regular Papers, Vol. 67, No. 9, pp.960-2971.
- 6. Manganiello, Patrizio, Mattia Ricco, Giovanni Petrone, Eric Monmasson and Giovanni Spagnuolo. "Optimization of perturbative PV MPPT methods through online system identification." IEEE Transactions on Industrial Electronics, Vol. 61, No. 12, pp. 6812-6821, 2014.
- Akash, J., V. Gomathi, S. Ajith Kumar and V. Chamundeeswari. "Comparative analysis of negative Luo converter and Cuk converter for harmonic reduction." In 2018 International Conference on Communication and Signal Processing (ICCSP), pp. 0532-0536, 2018.
- 8. Dheeban, S. S., Muthu Selvan NB and Umashankar Subramaniam. "Power conditioning of standalone Photo-voltaic system with BLDC motor by Negative-Output Luo Converter." In 2020 International Conference on Power Electronics and Renewable Energy Applications (PEREA), pp. 1-6. IEEE, 2020.
- 9. Thanzasankaran, R., ST Jaya Christa, J. Gnanavadivel and NiSenthil Kumar. "Design and analysis of negative output Luo Converter for Power Quality Enhancement." In 2018, International Conference on Current Trends towards Converging Technologies (ICCTCT), pp. 1-6, 2018.
- 10. Goudarzian, A and A. Khosravi. "Voltage regulation of a negative output Luo converter using a pd-pi type sliding mode current controller." International Journal of Engineering, Vol. 32, No. 2, pp. 277-285.
- 11. Nasiri, Hadi, Alireza Goudarzian and Navid Abjadi. "Design and implement a constant frequency sliding mode controller for a Luo converter." International Journal of Engineering, Vol. 29, No. 2, pp. 202-210, 2016.
- 12. Kayalvizhi, R., S. P. Natarajan, P. Suresh Pandiarajan and R. Vijayarajeswaran. "Control of paralleled negative output elementary Luo converters." In 2005 International Conference on Power Electronics and Drives Systems, Vol. 2, pp. 1234-1238, 2005.
- 13. Sivarajeswari, S and D. Kirubakaran. "Design and development of efficient Luo converters for DC microgrid." The International Journal of Electrical Engineering & Education, pp. 0020720919845152.
- 14. Li, Xun and Kwai Man Luk. "The grey wolf optimizer and its applications in electromagnetics." IEEE Transactions on Antennas and Propagation, Vol. 68, No. 3, pp. 2186-2197, 2019.
- Achiammal, B and R. Kayalvizhi. "Genetic algorithm based PI controller for negative output elementary luo converter."
   In 2014 IEEE International Conference on Advanced Communications, Control and Computing Technologies, pp. 1099-1103, 2014.
- 16. Nachammai, N., and R. Kayalvizhi. "Particle Swarm Optimized Fuzzy Controller for Luo Converter." International Journal of Engineering Research & Technology (IJERT), ISSN: 2278-0181, Vol. 6 Issue 10, pp.258-264, 2017
- 17. Yusubov, Elvin and Lala Bekirova. "A Moth-Flame optimized robust PID controller for a SEPIC in photovoltaic applications." IFAC-Papers Online, Vol. 55, No. 11, pp. 120-125, 2022.
- 18. Sahoo, Saroj Kumar, Apu Kumar Saha, Absalom E. Ezugwu, Jeffrey O. Agushaka, Belal Abuhaija, Anas Ratib Alsoud, and Laith Abualigah. "Moth flame optimization: theory, modifications, hybridizations, and applications." Archives of Computational Methods in Engineering, Vol. 30, No. 1, pp. 391-426, 2023.
- 19. Chincholkar, Satyajit H., Sangmesh V. Malge, and Sanjaykumar L. Patil. "Design and analysis of a voltage-mode non-linear control of a non-minimum-phase positive output elementary Luo converter." Electronics, Vol.11, No. 2, pp. 207-222, 2022.
- 20. Kumar, Rajan, and Bhim Singh. "Solar photovoltaic array fed Luo converter based BLDC motor driven water pumping system." In 2014 9th International Conference on Industrial and Information Systems (ICIIS), pp. 1-5, 2014.
- 21. Rajagopal, Veramalla, Danthurthi Sharath, Gundeboina Vishwas, Jampana Bangarraju, Sabha Raj Arya, and Challa Venkatesh. "Optimized controller gains using grey wolf algorithm for grid-tied solar power generation with improved dynamics and power quality." Chinese Journal of Electrical Engineering, Vol. 8, No. 2, pp. 75-85, 2022.
- 22. Valluru, Sudarshan K., Karan Sehgal, and Hitesh Thareja. "Evaluation of Moth-Flame Optimization, Genetic, and Simulated Annealing tuned PID controller for Steering Control of Autonomous Underwater Vehicle." In 2021 IEEE International IOT, Electronics and Mechatronics Conference (IEMTRONICS), pp. 1-6, 2021.
- 23. Singh, Bhim, and Radha Kushwaha. "Power factor preregulation in interleaved Luo converter-fed electric vehicle battery charger." IEEE Transactions on Industry Applications, Vol. 57, No. 3, pp. 2870-2882.
- 24. Singh, Bhim, Vashist Bist, Ambrish Chandra, and Kamal Al-Haddad. "Power factor correction in bridgeless-Luo converter-fed BLDC motor drive." IEEE Transactions on Industry Applications, Vol. 51, No. 2, pp. 1179-1188, 2014.
- 25. Aberoumandazar, Mehrdad, and Farzad Mohammadzadeh Shahir. "Stability analysis of Luo converter using state space modeling." Journal of Circuits, Systems and Computers, Vol. 30, No. 07, pp. 2150127-1-15, 2021.